

Superconductivity and phase diagram of $(\text{Li}_{0.8}\text{Fe}_{0.2})\text{OHFeSe}_{1-x}\text{S}_x$ X. F. Lu,^{1,2} N. Z. Wang,^{1,2} X. G. Luo,^{1,2,3} G. H. Zhang,^{4,5} X. L. Gong,⁶ F. Q. Huang,^{4,5} and X. H. Chen^{1,2,3,*}¹*Hefei National Laboratory for Physical Science at Microscale and Department of Physics, University of Science and Technology of China, Hefei, Anhui 230026, People's Republic of China*²*Key Laboratory of Strongly-Coupled Quantum Matter Physics, University of Science and Technology of China, Chinese Academy of Sciences, Hefei, Anhui 230026, People's Republic of China*³*Collaborative Innovation Center of Advanced Microstructures, Nanjing University, Nanjing 210093, People's Republic of China*⁴*CAS Key Laboratory of Materials for Energy Conversion, Shanghai Institute of Ceramics, Chinese Academy of Sciences, Shanghai 200050, People's Republic of China*⁵*Beijing National Laboratory for Molecular Sciences and State Key Laboratory of Rare Earth Materials Chemistry and Applications, College of Chemistry and Molecular Engineering, Peking University, Beijing 100871, People's Republic of China*⁶*CAS Key Laboratory of Mechanical Behavior and Design of Materials, Department of Modern Mechanics, University of Science and Technology of China, Hefei, Anhui 230027, People's Republic of China*

(Received 16 May 2014; revised manuscript received 2 December 2014; published 23 December 2014)

A series of $(\text{Li}_{0.8}\text{Fe}_{0.2})\text{OHFeSe}_{1-x}\text{S}_x$ ($0 \leq x \leq 1$) samples were successfully synthesized via hydrothermal reaction method and the phase diagram is established. Magnetic susceptibility suggests that an antiferromagnetism arising from $(\text{Li}_{0.8}\text{Fe}_{0.2})\text{OH}$ layers coexists with superconductivity, and the antiferromagnetic transition temperature nearly remains constant for various S doping levels. In addition, the lattice parameters of the both a and c axes decrease and the superconducting transition temperature T_c is gradually suppressed with the substitution of S for Se, and eventually superconductivity vanishes at $x = 0.90$. The decrease of T_c could be attributed to the effect of chemical pressure induced by the smaller ionic size of S relative to that of Se, being consistent with the effect of hydrostatic pressure on $(\text{Li}_{0.8}\text{Fe}_{0.2})\text{OHFeSe}$. But the detailed investigation on the relationships between T_c and the crystallographic facts suggests a very different dependence of T_c on anion height from the Fe2 layer or $Ch\text{-Fe2-}Ch$ angle from those in FeAs-based superconductors.

DOI: [10.1103/PhysRevB.90.214520](https://doi.org/10.1103/PhysRevB.90.214520)

PACS number(s): 74.70.Xa, 74.25.Dw, 74.25.-q

Since the discovery of superconductivity in $\text{LaFeAsO}_{1-x}\text{F}_x$ with $T_c \sim 26$ K [1], the iron-based superconductors, as the second family of compounds exhibiting high T_c after the cuprates, have attracted wide attention [2–4]. $\beta\text{-FeSe}$, which shows superconducting transition at ~ 10 K and owns the simplest crystal structure among iron-based superconductors, is thought to be a promising system to investigate the mechanism of high T_c superconductivity in iron-based superconductors [5]. By applying hydrostatic pressure or intercalating alkali atoms between FeSe layers (with chemical formula $A_x\text{Fe}_{2-y}\text{Se}_2$ [$A = \text{K, Rb, Cs, Tl/K, Tl/Rb, etc.}$], the T_c could be enhanced to higher than 30 K [6–10]. However, in $A_x\text{Fe}_{2-y}\text{Se}_2$, the obvious phase separation between the superconducting phase and the intergrown antiferromagnetic (AFM) insulating phase with an extremely high Néel temperature of ~ 560 K and Fe vacancy ordering [11–14], makes it difficult to study the underlying physics of FeSe layers. In addition, other FeSe-derived superconductors, such as alkali-metal ions and NH_3 molecules or organic-molecules intercalated FeSe [15–18], are extremely air sensitive, which prevents the further investigation of their physical properties. Thus, it is urgent to find other FeSe-derived superconductors with new spacer layers.

In iron-based superconductors, both carrier doping and isovalent substitution can tune the superconducting properties [4,19]. Similar to the external pressure effect, isovalent substitution would not change carrier density but could introduce

or enhance superconductivity, as found in the iron arsenides [19,20]. For instance, through substituting As with isovalent P, bulk superconductivity emerges in $\text{LaFeAs}_{1-x}\text{P}_x\text{O}$ with T_c of 10.8 K, which is understood in terms of chemical pressure and bond covalency [20]. However, in FeSe-derived superconductors $\text{K}_x\text{Fe}_{2-y}\text{Se}_{2-z}\text{S}_z$, the T_c is suppressed with S substituting for Se, and goes to zero at 80% of S, which has been attributed to the increase of Fe-Se tetrahedron irregularity and Fe1 site occupancy [21]. Recently, an air-stable FeSe-derived superconductor $(\text{Li}_{0.8}\text{Fe}_{0.2})\text{OHFeSe}$ was reported with T_c of ~ 40 K and the precise crystal structure has been unambiguously determined [22,23]. Moreover, there exists a canted AFM order originating from the $(\text{Li}_{0.8}\text{Fe}_{0.2})\text{OH}$ layer, which coexists with superconductivity. In this work, we report on the successful synthesis of $(\text{Li}_{0.8}\text{Fe}_{0.2})\text{OHFeSe}_{1-x}\text{S}_x$ ($0 \leq x \leq 1$) by using a hydrothermal reaction method. The evolution of superconducting properties and structure parameters with S content in $(\text{Li}_{0.8}\text{Fe}_{0.2})\text{OHFeSe}_{1-x}\text{S}_x$ are investigated. The results reveal that both a - and c -axis lattice parameters decrease almost linearly with the increase of S content. Superconductivity is suppressed by the substitution of S for Se, and finally vanishes at $x = 0.90$. Moreover, the AFM order locating within the $(\text{Li}_{0.8}\text{Fe}_{0.2})\text{OH}$ layer coexists with superconductivity, and the AFM transition temperature almost remains unchanged with S content.

A series of $(\text{Li}_{0.8}\text{Fe}_{0.2})\text{OHFeSe}_{1-x}\text{S}_x$ samples with nominal composition $x = 0.0\text{--}1.0$ were synthesized by a hydrothermal reaction method, as described in the previous report [22,23]. First, in order to ensure the reagents were fully dissolved and mixed, 0.012–0.02 mol selenourea (Alfa Aesar, 99.97% purity) and sulfourea (Sinopharm Chemical Reagent, A.R. purity)

*Corresponding author: chenxh@ustc.edu.cn

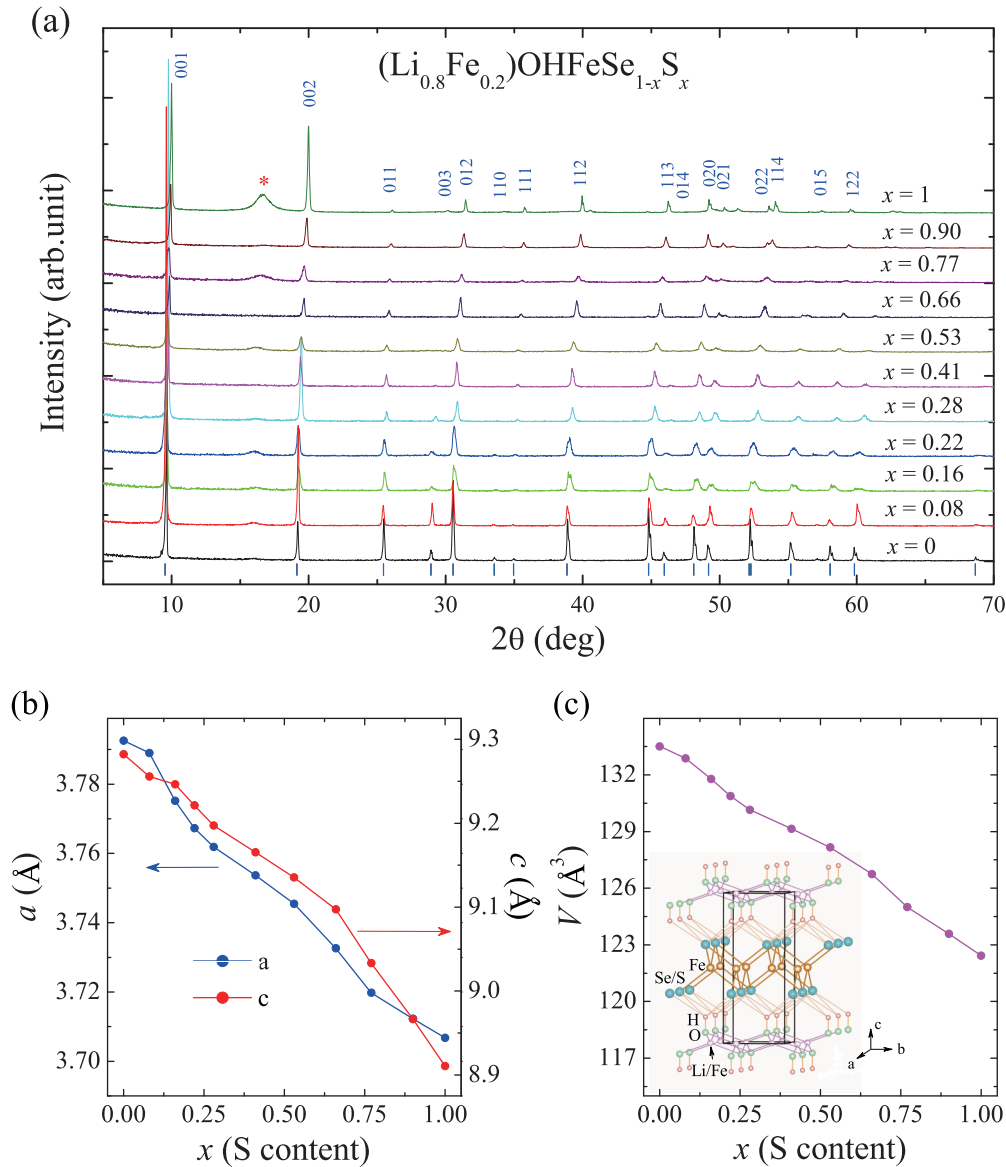


FIG. 1. (Color online) (a) The powder XRD patterns of $(\text{Li}_{0.8}\text{Fe}_{0.2})\text{OHFeSe}_{1-x}\text{S}_x$ ($0 \leq x \leq 1$) at room temperature. The asterisk represents the nanoscale FeS. (b) and (c) The lattice parameters of the a and c axes and unit cell volume as a function of the S content. The inset in (b) is the crystal structure of $(\text{Li}_{0.8}\text{Fe}_{0.2})\text{OHFeSe}_{1-x}\text{S}_x$ [23].

were stoichiometrically weighted, dissolved in 10 ml water, and stirred for 10–20 min in the Teflon-lined autoclave. Then 0.0075 mol Fe powder (Aladdin Industrial, A.R. purity) and 12 g $\text{LiOH}\cdot\text{H}_2\text{O}$ (Sinopharm Chemical Reagent, A.R. purity) were thrown into the autoclave and mixed. Finally, the Teflon-lined autoclave was tightly sealed and heated at 150–160 °C for 3–10 days. The polycrystalline samples acquired from the reaction systems were washed with deionized water repeatedly, and dried at room temperature.

Powder x-ray diffraction (XRD) data of samples were collected by using an x-ray diffractometer (SmartLab-9, Rigaku Corp.) with $\text{Cu } K\alpha$ radiation and a fixed graphite monochromator in the 2θ range of 5° – 70° at room temperature. The average stoichiometries of Fe, Se, and S of the polycrystalline samples were determined from energy-dispersive x-ray spectroscopy (EDX) analysis. The actual S contents x were determined by EDX to be 0, 0.08,

0.16, 0.22, 0.28, 0.41, 0.53, 0.66, 0.77, 0.90, and 1.0 for the 11 samples used in this work with the nominal molar reagents ratios of sulfourea/(sulfourea + selenourea) = 0, 0.1, 0.2, 0.3, 0.4, 0.5, 0.6, 0.7, 0.8, 0.9, and 1.0, respectively. Magnetization measurements were carried out on SQUID MPMS-XL5 (Quantum Design). Refinements of the XRD data were performed by using GSAS software [24,25].

Powder XRD patterns of $(\text{Li}_{0.8}\text{Fe}_{0.2})\text{OHFeSe}_{1-x}\text{S}_x$ samples are shown in Fig. 1(a), all of which were collected at room temperature. The XRD patterns of $(\text{Li}_{0.8}\text{Fe}_{0.2})\text{OHFeSe}_{1-x}\text{S}_x$ are similar to that of $(\text{Li}_{0.8}\text{Fe}_{0.2})\text{OHFeSe}$ and all reflections can be well indexed by the tetragonal structure on the basis of the space group of $P4/nmm$ (No. 129), except for the broad one at about $2\theta = 16^\circ$. The broad reflection at $2\theta \approx 16^\circ$ may be attributed to the nanoscale FeS produced in the low-temperature synthesis procedure [26]. As shown in Fig. 1(a), all reflections shift to the higher 2θ side with the increase

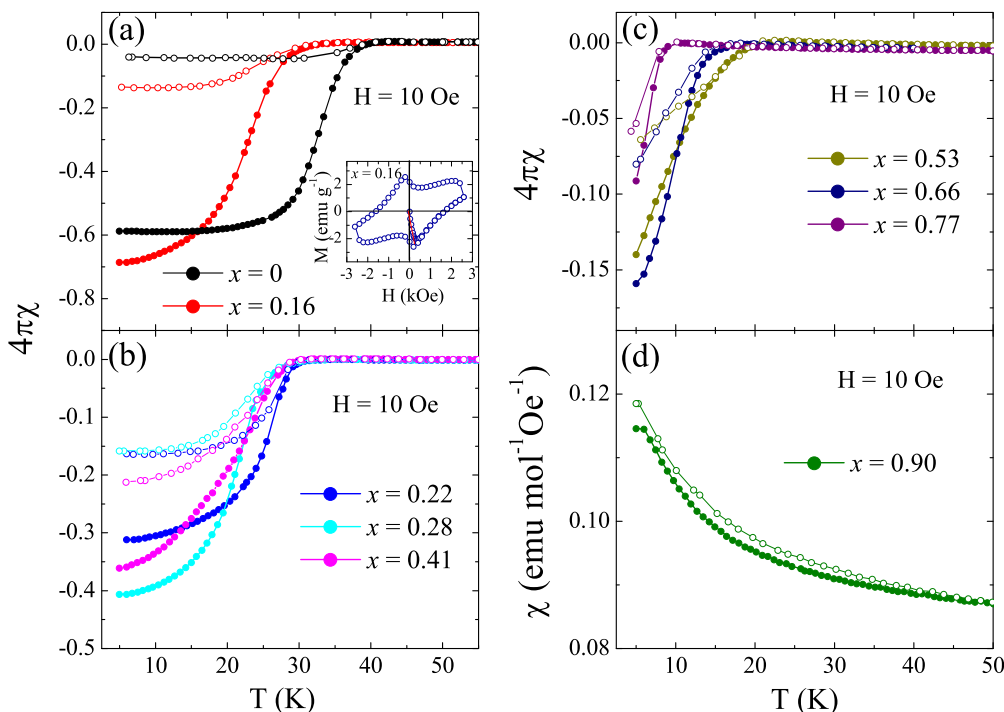


FIG. 2. (Color online) Temperature dependence of the dc magnetic susceptibility of the as-synthesized samples $(\text{Li}_{0.8}\text{Fe}_{0.2})\text{OHFeSe}_{1-x}\text{S}_x$, taken in zero-field-cooling (ZFC) (solid symbols) and field-cooling (FC) (open symbols) modes under an external field of 10 Oe. The inset of (a) is the M - H loop of $(\text{Li}_{0.8}\text{Fe}_{0.2})\text{OHFeSe}_{1-x}\text{S}_x$ ($x = 0.16$) taken at 5 K.

of S content. Figure 1(b) shows the evolution of the lattice parameters along the a and c axes as a function of S content x . With increasing x , the lattice parameters along both the a and c axes monotonically decrease, indicating the lattice contraction with increasing S content, which is consistent with the relatively smaller ionic size of S^{2-} compared with Se^{2-} . As a result, the unit cell volume $V = a \times a \times c$ also decreases monotonically. The lattice shrinking progressively with S substitution is consistent with Vegard's law, which is similar to $\text{K}_x\text{Fe}_{2-y}\text{Se}_{2-z}\text{S}_z$ and $\text{FeSe}_{1-x}\text{S}_x$ [21,27].

Figure 2 shows the temperature dependence of magnetic susceptibility χ for the superconducting samples under a magnetic field of 10 Oe. T_c determined from zero-field-cooling (ZFC) magnetic susceptibility shifts gradually to low temperature as the S content increases. When S content increases up to $x = 0.90$, no diamagnetic signal can be observed above 5 K and the temperature dependence of magnetic susceptibility shows paramagnetic behavior. Additionally, the shielding fractions at 5 K of $(\text{Li}_{0.8}\text{Fe}_{0.2})\text{OHFeSe}_{1-x}\text{S}_x$ ($x = 0.16$) estimated from the ZFC curves is 69%, suggesting a bulk superconductivity at 37 K. The M - H loop of the $x = 0.16$ sample measured at 5 K is presented in the inset of Fig. 2(a). A linear- H dependence of diamagnetic magnetization with negative slope can be observed up to ~ 150 Oe, which is in accordance with the superconducting transition observed in the temperature dependence of susceptibility. According to Mizuguchi's report [27], the S substitution in FeSe can stabilize the superconducting state. However, in our case, the sizes of crystalline grains from a low-temperature solution synthetic method are usually small and reduce the superconductive shielding fraction of samples, especially when x exceeds 0.50.

Figure 3 shows the temperature dependence of magnetic susceptibility χ for $x = 0$ and 0.28 samples from 2 to 300 K by applying an external field of 1 T. The superconductivity seemed to be suppressed under this field. However, the magnetic order in the $(\text{Li}_{0.8}\text{Fe}_{0.2})\text{OH}$ layer creates an internal field and completely suppresses the Meissner effect under 1 T. Thus, there is no diamagnetic signal observed under 1 T. Moreover, the temperature dependence of magnetization displays a Curie-Weiss behavior above 10 K. A sudden decrease in the χ happens in the ZFC curve around 8 K for both of the samples with $x = 0$ and 0.28. FC and ZFC magnetic susceptibilities bifurcate for both samples at about 8 K. The bifurcation is

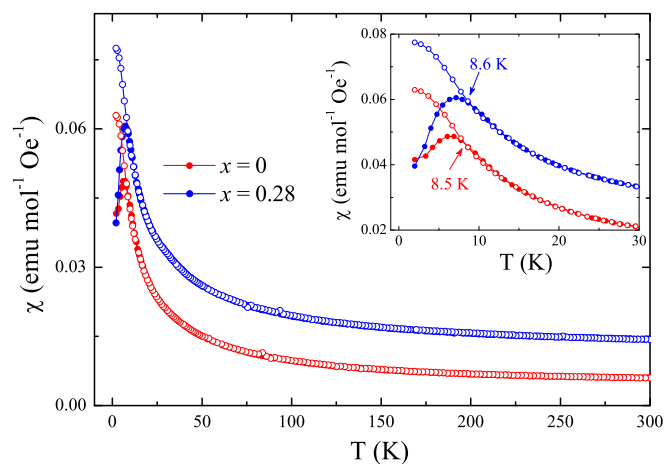


FIG. 3. (Color online) The temperature dependence of magnetic susceptibility χ for samples from 2 to 300 K by applying an external field of 1 T.

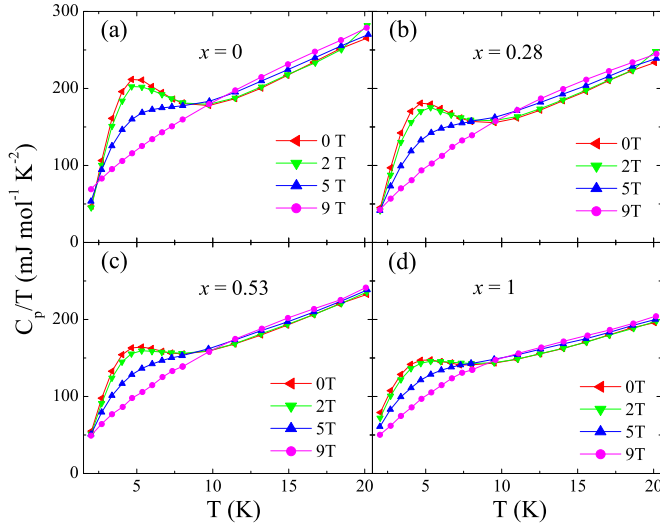


FIG. 4. (Color online) The specific heat of $(\text{Li}_{0.8}\text{Fe}_{0.2})\text{OHFeSe}_{1-x}\text{S}_x$ ($x = 0, 0.28, 0.53, 1.0$) under different external fields.

quite weak, suggesting a weak ferromagnetic component due to a possible canted antiferromagnetic order, as derived from nuclear magnetic resonance (NMR) measurements in other work [28]. The temperatures corresponding to the maximum of the ZFC susceptibility and the bifurcating temperature of ZFC and FC susceptibilities for the sample with $x = 0.28$ are almost the same as those observed in the S-free sample, strongly suggesting that this magnetic order is formed within the $(\text{Li}_{0.8}\text{Fe}_{0.2})\text{OH}$ layers, so that the substitution of S for Se cannot affect the magnetic transition. This is consistent with the NMR results in our other work, indicating that this magnetic ordered state originated from the $(\text{Li}_{0.8}\text{Fe}_{0.2})\text{OH}$ layers [28].

In order to confirm the AFM transition, we performed thermodynamic measurements. Figure 4 shows the specific heat measured under different magnetic fields. The specific heat for all the samples with different S contents begins to rise at about 8 K, which is consistent with the anomaly temperature

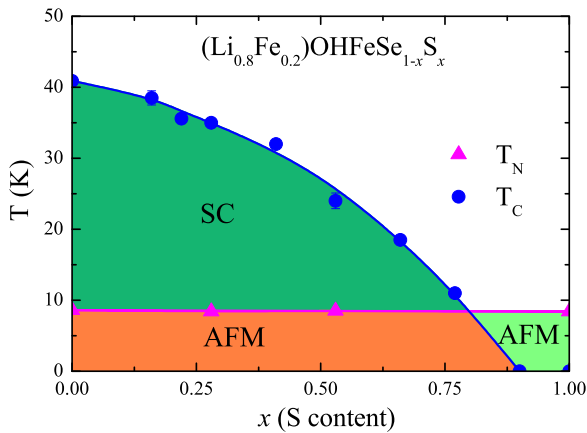


FIG. 5. (Color online) The phase diagram of $(\text{Li}_{0.8}\text{Fe}_{0.2})\text{OHFeSe}_{1-x}\text{S}_x$ derived from the magnetic susceptibility. The solid lines are a guide for the eye.

in the magnetic susceptibility. Such rise is suppressed with increasing magnetic fields and becomes very obscure as the field increases up to 9 T. Surprisingly, the temperature for the maximum of specific heat remains unshifted at 5 K in various magnetic fields. These features are consistent with the antiferromagnetic order proposed above. These results further suggest that the AFM ordering should arise from the $(\text{Li}_{0.8}\text{Fe}_{0.2})\text{OH}$ layer.

Based on the magnetic measurements displayed in Figs. 2 and 3 as well as the thermodynamic results shown in Fig. 4, the phase diagram is mapped out for the $(\text{Li}_{0.8}\text{Fe}_{0.2})\text{OHFeSe}_{1-x}\text{S}_x$ ($0 \leq x \leq 1$), as shown in Fig. 5, where T_c is determined by susceptibility and magnetic transition temperature is determined by the specific heat. The T_c gradually decreases and vanishes at $x = 0.90$, although the substituted S is isovalent to Se. The decrease of T_c is accompanied by the reduction of the a - and c -axis lattice parameters, suggesting the suppression effect of the chemical pressure on T_c . This is in accordance with the suppression effect of external pressure on superconductivity in $(\text{Li}_{0.8}\text{Fe}_{0.2})\text{OHFeSe}$.

It is believed that there are close relationships between T_c and crystallographic details. In our case, there is no other Fe site between the $(\text{Li}_{0.8}\text{Fe}_{0.2})\text{OH}$ layer and the $\text{FeSe}_{1-x}\text{S}_x$ layer, and both the chalcogen (Ch) anion height from the Fe2 layer and the $\text{Fe2-}Ch$ bond distance in $\text{FeSe}_{1-x}\text{S}_x$ slab monotonically decrease with increasing S content, as shown in Fig. 6(a). The evolution of the Ch -Fe2- Ch angle in the Fe2- Ch tetrahedron is shown in Fig. 6(b). The Ch -Fe2- Ch angles change towards the ideal value of a regular tetrahedron (109.47°). According to a previous report [29], T_c is closely connected to the anion height from the Fe layer (h) and a maximum T_c could be achieved with $h_0 \approx 1.38 \text{ \AA}$ for FeAs-derived superconductors. For the FeSe-derived superconductors, the anion height dependence of T_c has been established as a V shape [22] with a minimum T_c at $h = 1.45 \text{ \AA}$ [22], distinct from the inverse V-shaped one in FeAs-based superconductors. Both S and Te substitutions for Se in FeSe would enhance T_c [27,30], which could be attributed to the variation of anion height and follow the law of V-shape dependence of T_c . However, in regard to $\text{K}_x\text{Fe}_{2-y}\text{Se}_{2-z}\text{S}_z$, the anion height dependence of T_c violates this law, which can be explained in terms of the existence of the Fe vacancies, which results in a nonmonotonic change of the anion height with S content [21]. In Fig. 6(c), we plot T_c as a function of chalcogen height from the Fe layer for $(\text{Li}_{0.8}\text{Fe}_{0.2})\text{OHFeSe}_{1-x}\text{S}_x$, which shows that the T_c is monotonically decreased with shrinking of the anion height from the Fe layer, with no sudden change in slope at $h = 1.38$ or 1.45 \AA . This does not follow the previous V shape in FeSe-derived superconductors or the inverse V shape in FeAs-based superconductors, suggesting the existence of peculiar physics in the $(\text{Li}_{0.8}\text{Fe}_{0.2})\text{OHFeSe}_{1-x}\text{S}_x$ system. In FeAs-based superconductors, it is also thought that the regular tetrahedron of FeAs_4 might favor higher T_c and this might hold in FeSe-derived superconductors. However, Fig. 6(d) shows that T_c decreases monotonically as the Ch -Fe2- Ch angle goes to the ideal value of a regular tetrahedron, implying that a tetrahedron distortion in FeSe-derived superconductors may promote the superconductivity.

Another intriguing phenomenon of the phase diagram shown in Fig. 5 is that although the T_c can be effectively

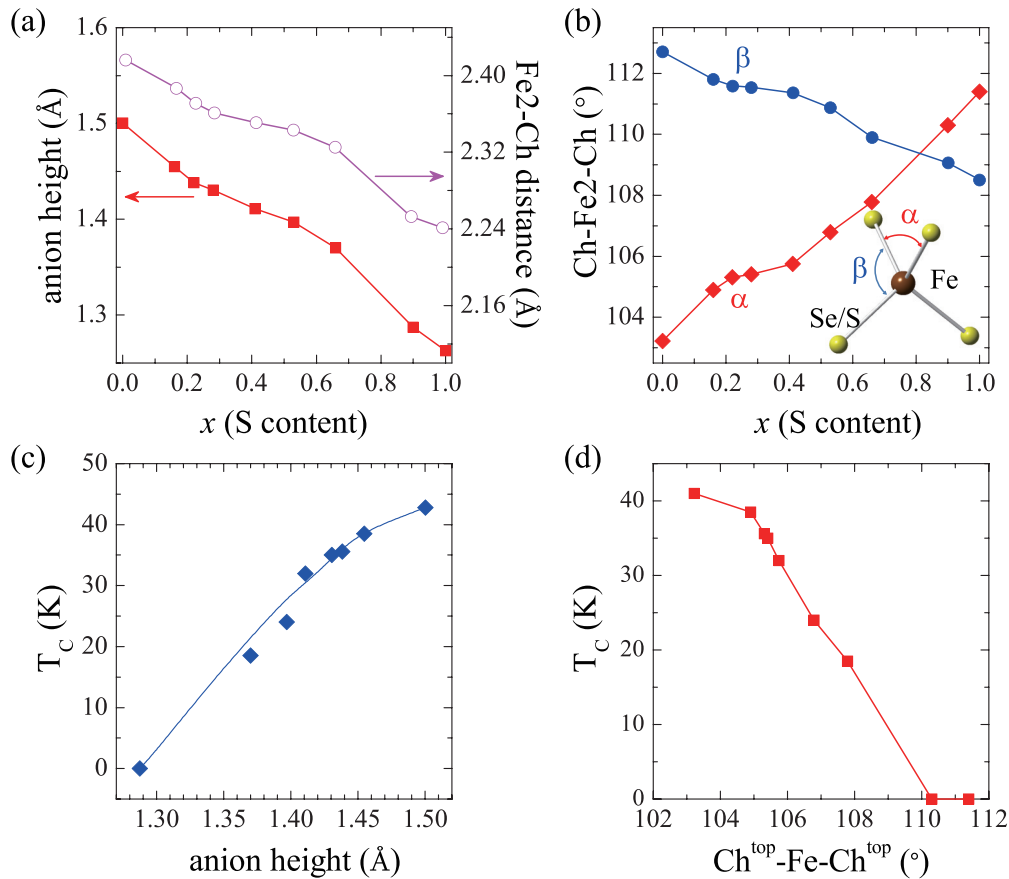


FIG. 6. (Color online) (a) and (b) The evolution of Ch -Fe2- Ch angles (2 \times and 4 \times) and Fe2- Ch bond lengths in the Fe2- Ch tetrahedron and the anion height from the Fe2 layer with S substitution, where Ch is the chalcogen S and Se. (c) T_c plotted against chalcogen anion height for $(\text{Li}_{0.8}\text{Fe}_{0.2})\text{OHFeSe}_{1-x}\text{S}_x$ ($0 \leq x \leq 1$) samples. (d) The relationship between T_c and Ch -Fe2- Ch angles (2 \times).

suppressed by S substitution, the AFM transition temperature remains almost unchanged. In the superconducting region of S content, AFM ordering exists deeply inside the superconducting state and coexists with superconductivity in the whole region, but seems to have no connection with the superconductivity. For a conventional superconductor, local magnetic moments or magnetic order is usually unfavorable to superconductivity. However, AFM order from $(\text{Li}_{0.8}\text{Fe}_{0.2})\text{OH}$ layers seems not to affect superconductivity occurring in the conducting FeSe layers for $(\text{Li}_{0.8}\text{Fe}_{0.2})\text{OHFeSe}_{1-x}\text{S}_x$. Actually, it is found in FeAs-based superconductors that magnetism or magnetic moments outside the conducting FeAs layers can have negligible suppression effect on superconductivity. In $\text{Eu}_{1-x}\text{La}_x\text{Fe}_2\text{As}_2$, AFM can also exist deep inside the superconducting region with both T_c and AFM transition temperature increasing with enhancing external pressure [31]. Replacement of magnetic Nd, Pr, Sm, and Gd for nonmagnetic La in $\text{LaFeAsO}_{1-x}\text{F}_x$ or $\text{LaFeAsO}_{1-\delta}$ can enhance T_c effectively [2,3,32,33]. These facts strongly manifest the unconventional superconductivity in the Fe-based superconductors. It also suggests that the correlation along the c axis plays a trivial role in the superconductivity in the Fe-based superconductors.

In summary, we successfully synthesized a series of $(\text{Li}_{0.8}\text{Fe}_{0.2})\text{OHFeSe}_{1-x}\text{S}_x$ ($0 \leq x \leq 1$) samples through the hydrothermal method. Due to the smaller ionic size of S

relative to that of Se, the S substitution leads to shrinking of the lattice parameters both along the a axis and the c axis. Magnetic susceptibility and specific heat were also studied. Based on the magnetic susceptibility and thermodynamic results of all the samples, the phase diagram of $(\text{Li}_{0.8}\text{Fe}_{0.2})\text{OHFeSe}_{1-x}\text{S}_x$ is mapped out. T_c is suppressed from 40 K to zero as S content increases from 0 to 0.90. The effect of chemical pressure resulting from S substitution for Se is considered as a possible mechanism of the suppression of T_c , which is in agreement with the effect of external pressure previously investigated in $(\text{Li}_{0.8}\text{Fe}_{0.2})\text{OHFeSe}$. But the relationships between T_c and the crystallographic details reveal that the dependence of T_c on anion height from the Fe2 layer or the Ch -Fe2- Ch angle is distinct from those summarized in FeAs-based superconductors. Magnetic susceptibility at 1 T and the specific heat suggest that an AFM transition around 8 K originates from $(\text{Li}_{0.8}\text{Fe}_{0.2})\text{OH}$ layers. The magnetic transition temperature does not alter with S concentration, and superconductivity coexists with antiferromagnetism in the superconducting region of S content.

This work is supported by the National Natural Science Foundation of China (China) (Grants No. 11190021, No. 11174266, and No. U1330105), the ‘‘Strategic Priority Research Program(B)’’ of the Chinese Academy of Sciences (China) (Grant No. XDB04040100), the National Basic Research Program of China (China) (973 Program, Grants

No. 2012CB922002 and No. 2011CBA00101), National Key Project of Magneto-Restriction Fusion Energy Development

Program (Grant No. 2013GB110002), and the Chinese Academy of Sciences.

-
- [1] Y. Kamihara, T. Watanabe, M. Hirano, and H. Hosono, *J. Am. Chem. Soc.* **130**, 3296 (2008).
- [2] X. H. Chen, T. Wu, G. Wu, R. H. Liu, H. Chen, and D. F. Fang, *Nature (London)* **453**, 761 (2008).
- [3] Z. A. Ren, G. C. Che, X. L. Dong, J. Yang, W. Lu, W. Yi, X. L. Shen, Z. C. Li, L. L. Sun, F. Zhou, and Z. X. Zhao, *Europhys. Lett.* **83**, 17002 (2008).
- [4] M. Rotter, M. Tegel, and D. Johrendt, *Phys. Rev. Lett.* **101**, 107006 (2008).
- [5] F. C. Hsu, J. Y. Luo, K. W. Yeh, T. K. Chen, T. W. Huang, P. M. Wu, Y. Y. Lee, Y. L. Huang, Y. Y. Chu, D. C. Yan, and M. K. Wu, *Proc. Natl. Acad. Sci. USA* **105**, 14262 (2008).
- [6] S. Medvedev, T. M. McQueen, I. A. Troyan, T. Palasyuk, M. I. Erements, R. J. Cava, S. Naghavi, F. Casper, V. Ksenofontov, G. Wortmann, and C. Felser, *Nat. Mater.* **8**, 630 (2009).
- [7] J. G. Guo, S. F. Jin, G. Wang, S. C. Wang, K. X. Zhu, T. T. Zhou, M. He, and X. L. Chen, *Phys. Rev. B* **82**, 180520(R) (2010).
- [8] A. F. Wang, J. J. Ying, Y. J. Yan, R. H. Liu, X. G. Luo, Z. Y. Li, X. F. Wang, M. Zhang, G. J. Ye, P. Cheng, Z. J. Xiang, and X. H. Chen, *Phys. Rev. B* **83**, 060512(R) (2011).
- [9] A. Krzton-Maziopa, Z. Shermadini, E. Pomjakushina, V. Pomjakushin, M. Bendele, A. Amato, R. Khasanov, H. Luetkens, and K. Conder, *J. Phys.: Condens. Matter* **23**, 052203 (2011).
- [10] M. H. Fang, H. D. Wang, C. H. Dong, Z. J. Li, C. M. Feng, J. Chen, and H. Q. Yuan, *Europhys. Lett.* **94**, 27009 (2011).
- [11] W. Li, H. Ding, P. Deng, K. Chang, C. L. Song, K. He, L. L. Wang, X. C. Ma, J. P. Hu, X. Chen, and Q. K. Xue, *Nat. Phys.* **8**, 126 (2012).
- [12] W. Bao, Q. Z. Huang, G. F. Chen, M. A. Creen, D. M. Wang, J. B. He, and Y. M. Qiu, *Chin. Phys. Lett.* **28**, 086104 (2011).
- [13] W. Bao, G. N. Li, Q. Z. Huang, G. F. Chen, J. B. He, D. M. Wang, M. A. Green, Y. M. Qiu, J. L. Luo, and M. M. Wu, *Chin. Phys. Lett.* **30**, 027402 (2013).
- [14] Z. W. Wang, Z. Wang, Y. J. Song, C. Ma, Y. Cai, Z. Chen, H. F. Tian, H. X. Yang, G. F. Chen, and J. Q. Li, *J. Phys. Chem. C* **116**, 17847 (2012).
- [15] T. P. Ying, X. L. Chen, G. Wang, S. F. Jin, T. T. Zhou, X. F. Lai, H. Zhang, and W. Y. Wang, *Sci. Rep.* **2**, 426 (2012).
- [16] M. Burrard-Lucas, D. G. Free, S. J. Sedlmaier, J. D. Wright, S. J. Cassidy, Y. Hara, A. J. Corkett, T. Lancaster, P. J. Baker, S. J. Blundell, and S. J. Clarke, *Nat. Mater.* **12**, 15 (2013).
- [17] E.-W. Scheidt, V. R. Hathwar, D. Schmitz, A. Dunbar, W. Scherer, F. Mayr, V. Tsurkan, J. Deisenhofer, and A. Loidl, *Eur. Phys. J. B* **85**, 279 (2012).
- [18] A. Krzton-Maziopa, E. V. Pomjakushina, V. Y. Pomjakushin, F. Rohr, A. Schilling, and K. Conder, *J. Phys.: Condens. Matter* **24**, 382202 (2012).
- [19] S. Jiang, H. Xing, G. F. Xuan, C. Wang, Z. Ren, C. M. Feng, J. H. Dai, Z. A. Xu, and G. H. Cao, *J. Phys.: Condens. Matter* **21**, 382203 (2009).
- [20] C. Wang, S. Jiang, Q. Tao, Z. Ren, Y. Li, L. Li, C. Feng, J. Dai, G. Cao, and Z. A. Xu, *Europhys. Lett.* **86**, 47002 (2009).
- [21] H. C. Lei, M. Abeykoon, E. S. Bozin, K. F. Wang, J. B. Warren, and C. Petrovic, *Phys. Rev. Lett.* **107**, 137002 (2011).
- [22] X. F. Lu, N. Z. Wang, G. H. Zhang, X. G. Luo, Z. M. Ma, B. Lei, F. Q. Huang, and X. H. Chen, *Phys. Rev. B* **89**, 020507(R) (2014).
- [23] X. F. Lu, N. Z. Wang, H. Wu, Y. P. Wu, D. Zhao, X. Z. Zeng, X. G. Luo, T. Wu, W. Bao, G. H. Zhang, F. Q. Huang, Q. Z. Huang, and X. H. Chen, *Nat. Mater.*, doi:10.1038/nmat4155 (2014).
- [24] A. C. Larson and R. B. Von Dreele, Los Alamos National Laboratory Report LAUR 86-748, 1994.
- [25] B. H. Toby, *J. Appl. Crystallogr.* **34**, 210 (2001).
- [26] A. R. Lennie and D. J. Vaughan, in *Mineral Spectroscopy: A Tribute to Roger G. Burns*, edited by M. D. Dyar, C. McCammon, and M. W. Schaefer (The Geochemical Society, Houston, 1996), p. 117.
- [27] Y. Mizuguchi, F. Tomioka, S. Tsuda, T. Yamaguchi, and Y. Takano, *J. Phys. Soc. Jpn.* **78**, 074712 (2009).
- [28] Y. P. Wu *et al.* (unpublished).
- [29] Y. Mizuguchi, Y. Hara, K. Deguchi, S. Tsuda, T. Yamaguchi, K. Takeda, H. Kotegawa, H. Tou, and Y. Takano, *Supercond. Sci. Technol.* **23**, 054013 (2010).
- [30] K.-W. Yeh, T. W. Huang, Y. L. Huang, T. K. Chen, F. C. Hsu, P. M. Wu, Y. C. Lee, Y. Y. Chu, C. L. Chen, J. Y. Luo, D. C. Yan, and M. K. Wu, *Europhys. Lett.* **84**, 37002 (2008).
- [31] M. Zhang, J. J. Ying, Y. J. Yan, A. F. Wang, X. F. Wang, Z. J. Xiang, G. J. Ye, P. Cheng, X. G. Luo, J. P. Hu, and X. H. Chen, *Phys. Rev. B* **85**, 092503 (2012).
- [32] Z. A. Ren, W. Lu, J. Yang, W. Yi, X. L. Shen, Z. C. Li, G. C. Che, X. L. Dong, L. L. Sun, F. Zhou, and Z. X. Zhao, *Chin. Phys. Lett.* **25**, 2215 (2008).
- [33] Z. A. Ren, J. Yang, W. Lu, W. Yi, X. L. Shen, Z. C. Li, G. C. Che, X. L. Dong, L. L. Sun, F. Zhou, and Z. X. Zhao, *Europhys. Lett.* **82**, 57002 (2008).